Experimental Investigation of Shear Transfer in Exposed Column Base Connections

IVAN R. GOMEZ, AMIT M. KANVINDE and GREGORY G. DEIERLEIN

ABSTRACT

Shear transfer mechanisms in exposed column base plate connections are examined through a series of seven full-scale tests. Three mechanisms of shear transfer are investigated, including friction between the base plate and grout support, anchor rod flexure and shear, and shear key (shear lug) bearing. Seven tests were conducted on relatively large-scale specimens that reflect the common base connection configurations as described in the American Institute of Steel Construction's (AISC) *Steel Design Guide 1: Base Plate and Anchor Rod Design.* A coefficient of friction equal to 0.46 was measured from three tests investigating friction transfer mechanisms between the steel base plate and grout pad, which is comparable to the design value (0.40) specified by the American Concrete Institute for friction between as-rolled steel and concrete. Two tests investigating anchor rod bearing provided data to evaluate the shear resistance provided by a combination of axial tension, shear and flexure, wherein the anchor rods bend in reverse curvature over a distance roughly equal to the base plate thickness plus one-half of the thickness of the welded plate washer. This strength capacity prediction is consistent with a method outlined by the AISC *Steel Design Guide 1*. Failure of the concrete footing due to edge breakout was investigated as a limit state for shear lug bearing. Data from two tests indicate that for large footings, the current AISC *Steel Design Guide 1* procedures, adapted from the American Concrete Institute, may be unconservative due to the size effect in concrete, which reduces the available shear capacity for larger structure geometries. A method that incorporates the size effect is shown to provide a more accurate assessment of the free-edge breakout strength of the concrete. Limitations of the study and future areas of work are outlined.

Keywords: base plates, anchor rods, column base connections, shear key, shear transfer.

Most previous studies on column base plate connections have focused on response that is controlled by axial force (DeWolf, 1978) or combined axial force and flexure (DeWolf and Sarisley, 1980; Astaneh and Bergsma, 1993). There is comparatively limited published research on shear transfer mechanisms through exposed column base connections. Current design guidelines for shear transfer (Fisher and Kloiber, 2006) are generally based on adaptations of test data from idealized small-scale components that may not necessarily represent the actual conditions present in column base connections. For example, many studies have investigated friction behavior between steel and concrete or grout (Rabbat and Russell, 1985). However, no documented studies examine configurations that reflect common column base construction, such as the use of steel shim stacks for column erection. Similarly, several studies have addressed the response of anchor rods embedded in concrete. However, most studies address failure modes of the concrete (rather than the anchor itself) such as rod pullout or concrete breakout (Klingner et al., 1982). These existing studies do not reflect typical conditions in column base connections, where the shear load is introduced into the anchor rods through welded plate washers, such that the rods may be subjected to a combination of axial and shear forces, as well as bending.

The objective of this study is to characterize shear transfer in steel column base connections through the development of mechanics-based models that are supported by test data. Referring to the details shown in Figure 1, the study focuses on "exposed" column base connections. In contrast to embedded base connections, wherein the column is embedded in the footing, exposed connections are installed on the surface of the foundation and thus cannot benefit from shear (or flexural) resistance from the concrete surrounding the embedment. This study includes seven large-scale tests to characterize the following three shear transfer mechanisms in exposed column base plates: (1) friction between the steel base plate and supporting grout base, (2) anchor rod bearing and (3) shear key (shear lug) bearing. These three mechanisms represent popular design alternatives for the design of base plates subjected to shear loading in exposed column base plate connections (Fisher and Kloiber, 2006). The tests are devised to isolate each of these three mechanisms, which are characterized through the application of shear loading in the presence of axial compression or tension.

Ivan R. Gomez, Ph.D., Research Engineer, AIR Worldwide Corporation, San Francisco, CA 94111. E-mail: igomez@air-worldwide.com

Amit M. Kanvinde, Ph.D., Associate Professor, Department of Civil and Environmental Engineering, University of California, Davis, CA 95618. E-mail: kanvinde@ucdavis.edu

Gregory G. Deierlein, Ph.D., P.E., Professor, Department of Civil and Environmental Engineering, Stanford University, Stanford, CA 94305. E-mail: ggd@stanford.edu

BACKGROUND, OBJECTIVES AND SCOPE

The American Institute of Steel Construction's (AISC) *Steel Design Guide 1*, along with its referenced codes and standards, form the design basis for steel column bases in the United States. The first edition of the AISC *Steel Design Guide 1—Column Base Plates* (DeWolf and Ricker, 1990) outlined procedures for the design of column base connections, including bases subjected to axial compression and flexure. AISC *Steel Design Guide 1* cited the lack of design provisions and test data to characterize shear transfer mechanisms. The report referenced a few of the available publications on shear transfer in base plates, most of which are based on analytical research (Ballio and Mazzolani, 1983; Goldman, 1983; Shipp and Haninger, 1983; Tronzo, 1984). The second (and current) edition of the AISC *Steel Design Guide 1* (Fisher and Kloiber, 2006) includes additional information on shear transfer, including a more comprehensive treatment of anchor rod and shear key design for shear loading. These provisions are based to a large extent on existing information from several guidelines and standards, including the AISC *Steel Construction Manual* (AISC, 2005a) and the American Concrete Institute (ACI) *Manual of Concrete Practice* (ACI 318, 2008; ACI 349, 2006). Design provisions for column base connections have also been proposed in other standards, including guidance for earthquake-resistant design in the AISC *Seismic Provisions for Structural Steel Buildings* (AISC, 2005b) and the Occupational Safety and Health Administration (OSHA, 2001). Literature reviews by the authors (Gomez et al., 2009) and others (Grauvilardell et al., 2005) summarize most of the available information on the design and behavior of exposed steel column base connections.

With respect to force transfer through surface friction (see Figure 1b), various studies (Rabbat and Russell, 1985; Baltay and Gjelsvik, 1990; Cook and Klingner, 1992; Nagae et al., 2006) have reported average friction coefficient values in the range of 0.43 to 0.70 for slip surfaces between steel and concrete or steel and grout. However, these studies examine small-scale components and do not account for the presence of shim stacks under the base plate, which may affect frictional response. Only Nagae et al. (2006) considers the evolution of friction under reversed cyclic loading.

Various studies have investigated the response of anchor rods and steel anchorages in concrete, such as shown in Figure 1c. Many of these emphasize failure of either the grout or the concrete in the vicinity of the anchor rod either due to pullout, localized crushing or free-edge breakout (Conrad, 1969; Cannon et al., 1975; Bailey and Burdette, 1977; Cannon et al., 1981; Klingner et al., 1982). Design considerations developed from these studies mainly address anchorage lengths, edge distances and reinforcement details and have been adopted into concrete design codes (e.g., ACI 318). Fuchs et al. (1995) developed the concrete capacity design (CCD) method, which is currently the preferred approach for the concrete design of embedded fasteners under shear or tensile loading (see Appendix D in ACI 318-08). Adihardjo and Soltis (1979) and Nakashima (1998) investigated the response of anchor rods in grouted base plates. However, their investigations were limited to single rod components tested under shear and tensile forces. Recent work by Gresnigt et al. (2008) presents test data in support of their development of analytical models for anchor rod bearing in column bases subjected to combined monotonic shear and tension forces. However, their test specimens did not include base plates with oversized anchor rod holes commonly used in the United States.

Shear keys, consisting of a plate or stub beam welded to the underside of the base plate and embedded within the concrete footing (see Figure 1d) can be effective to resist moderate to high shear forces. In addition to the possible failure of the shear key itself, the primary failure modes associated with force transfer through a shear key include (1) concrete bearing failure directly in front of the shear key, in which a wedge-like failure surface develops in the concrete footing directly in front of the shear key, and (2) free-edge breakout failure of the concrete footing. Design provisions for failure mode 1 are provided in ACI 349 (2006) and are based on tests by Rotz and Reifschneider (1989). In addition, the bearing strength of concrete has been previously investigated by Hawkins (1968). However, to the authors' knowledge, test data have not been published for concrete free-edge breakout from shear keys in base connections. Nevertheless, ACI 349 (2006) and the AISC *Steel Design Guide 1* (Fisher and Kloiber, 2006) outline a method to calculate the breakout shear capacity of shear lugs loaded toward a free edge. This method, which is commonly referred to as the 45° cone method, assumes a uniform tensile stress acting on the projected area of an assumed failure wedge. The general design method for concrete embedments (refer to Appendix D in ACI 318-08), referred to as the concrete capacity design (CCD) method, is similar, except that it incorporates the size effect in concrete (Bažant, 1984). The size effect predicts lower unit strength for large concrete footings, because failure may be initiated by fracture, rather than the mobilization of a uniform stress over the entire breakout surface. Both of these methods address the design of concrete elements, rather than the shear key itself.

As outlined previously, there are several significant gaps in knowledge and supporting test data to characterize shear transfer mechanisms in column base connections. With the goal to evaluate and improve design models for shear transfer, seven large-scale column base connections were tested and analyzed. The tests focus on exposed base plate connection details, shown in Figure 1a, and the three shear force transfer mechanisms illustrated in Figures 1b, 1c and 1d, with the following objectives:

1. **Surface friction:** Characterize the coefficient of friction between the steel base plate and underlying grout fill under cyclic shear loading for realistic column base plate details, including the presence of leveling shim stacks beneath the base plate.

2. **Anchor rod bearing:** Characterize the strength of base plate anchor rods under the combination of axial tension, shear and flexure. An important issue in this regard is the accurate characterization of the effective bending length and bending shape of the anchor rod.

3. **Shear key bearing:** Investigate the strength capacity associated with the free-edge breakout of an unreinforced concrete footing due to an embedded shear key.

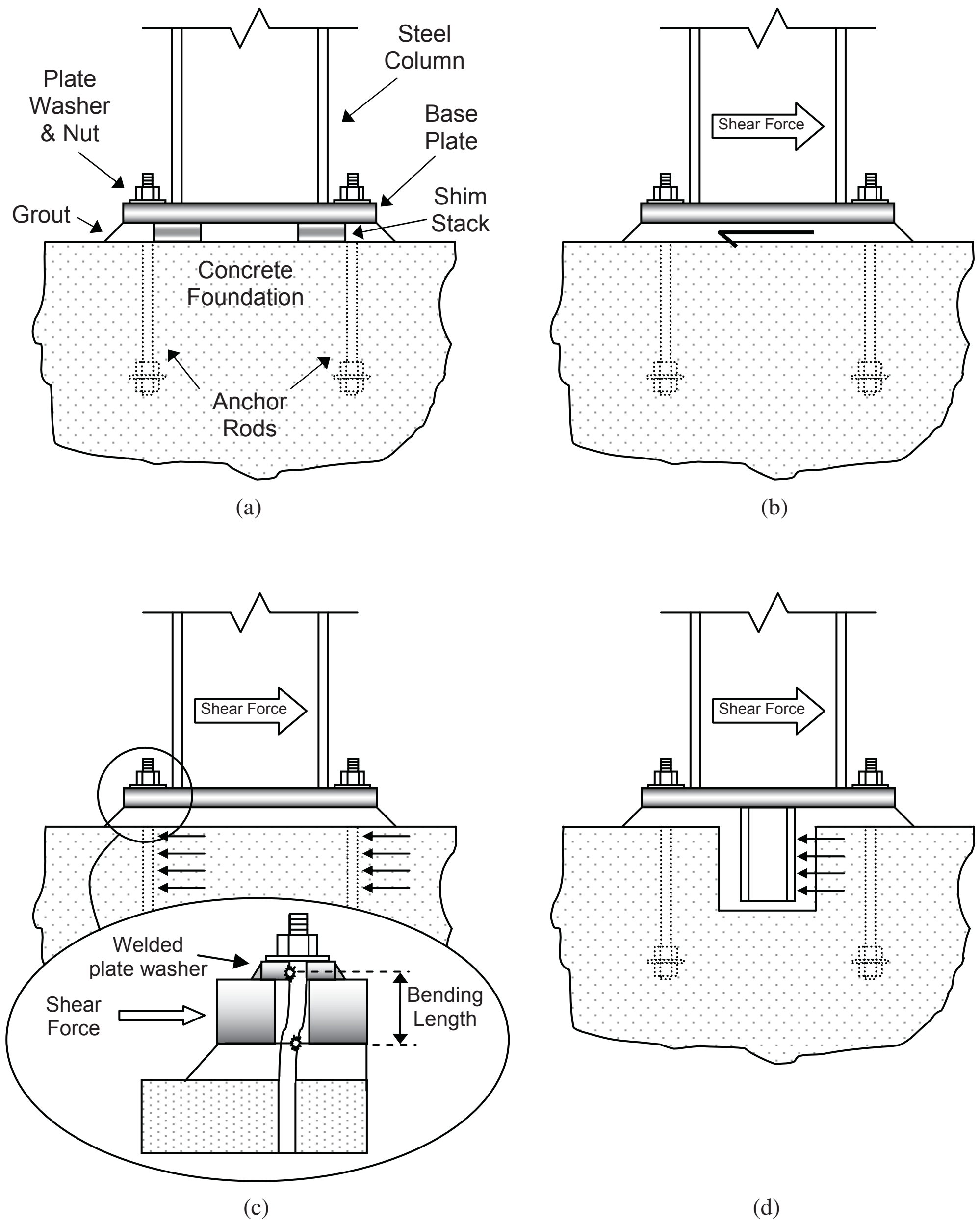

Fig. 1. Typical exposed column base connections and associated shear transfer mechanisms: (a) base plate detail; (b) surface friction; (c) anchor rod bearing; (d) shear key bearing. (Adapted from the 2005 AISC Seismic Provisions)

Table 1. Test Matrix, Test Results and Strength Estimates								
Test	**Mechanism**	**Test Detail**	**Loading Description**	**μ**	**$V_{measured}$, kips[a]**		**V_{calc} (1), kips[b]**	**V_{calc} (2), kips[b]**
1	Surface friction	Representative shim stacks	Cyclic shear with axial compression of 43 kips, 112 kips and 261 kips	0.40	N.A.			
2				0.48				
3		Grout only		0.46				
4	Anchor rod bearing	¾-in.-diameter anchor rods	Cyclic shear with 40 kips axial tension	N.A.	Fwd.	30.2	11.4	26.5
					Rev.	28.2		
					Avg.	**29.2**		
5		1¼-in.-diameter anchor rods	Cyclic shear with 108 kips axial tension		Fwd.	126	36.9	75.3
					Rev.	70.4		
					Avg.	**98.2**		
6	Shear key bearing	5.5-in. embedment depth	Monotonic shear with small axial compression		Fwd.	193	318	144
					Rev.	159		
					Avg.	**176**		
7		3.0-in. embedment depth			Fwd.	142	302	151
					Rev.	136		
					Avg.	**139**		

[a] Peak ultimate measured force in forward and reverse loading direction and average of both.
[b] Calculated strengths as defined in the text.

TEST PROGRAM AND RESULTS

Following the objectives as just outlined, seven large-scale column base connection specimens were tested. As outlined in Table 1, the program included three tests to evaluate shear transfer through friction (Figure 1b), two tests of shear transfer through anchor rod bearing (Figure 1c) and two tests of shear transfer through shear keys (Figure 1d). These mechanisms represent popular design alternatives for shear transfer in exposed base plate connections and are discussed in the AISC *Steel Design Guide 1* (Fisher and Kloiber, 2006). Referring to Table 1, surface friction is examined under cyclic shear and three levels of compression axial load. Two of the surface friction specimens (tests 1 and 2) include steel shim stacks beneath the base plate to reflect common construction details, whereas the third specimen (test 3) does not have shim stacks. Tests 4 and 5 had anchor rods of ¾-in.- and 1¼-in.-diameter, respectively, with welded plate washers which transferred shear through combined shear and bending in the rods. The shear keys of tests 6 and 7 had embedment depths of 5.5 in. and 3.0 in., respectively, below the concrete surface and were tested in monotonic shear. The specimens were prepared in accordance with the AISC *Steel Design Guide 1* (Fisher and Kloiber, 2006) to reflect common construction practice, such as the use of high-strength, non-shrink general construction grout (see Gomez et al., 2009, for further details).

The testing apparatus and a photograph of the base plate detail are shown in Figure 2, and a plan view of the column base plate and concrete footing is shown in Figure 3. The large cruciform-shaped loading frame transferred compressive and tensile axial loads from the vertical actuators to the base plate, and horizontal shear load was applied through assemblies bolted directly onto the base plate. Thus, the apparatus allowed the application of direct shear and axial forces with negligible moment at the base connection. The test assembly, including the 2-in.-thick base plate, was designed to remain undamaged during testing and was reused (with minor modifications) for all seven tests. Applied loads were measured through load cells on each actuator, and the weight of the test rig (17 kips) was subtracted from the axial loads to determine the net axial load applied to the base plate. As indicated in Figure 3, the base plate was larger than the grout fill area to accommodate attachment of the horizontal actuators. For the friction tests, the grout fill area was smaller than in the other tests to allow for the application of bearing stresses consistent with working loads in a building (up to 400 psi). The nonstandard column size (W31×191) was selected such that the cruciform-shaped loading frame was highly rigid to minimize rotational deformations at the base plate.

Loading Protocols

While established loading protocols are available for testing of deformation-sensitive components such as beam-column connections (Krawinkler et al., 2000), similar protocols

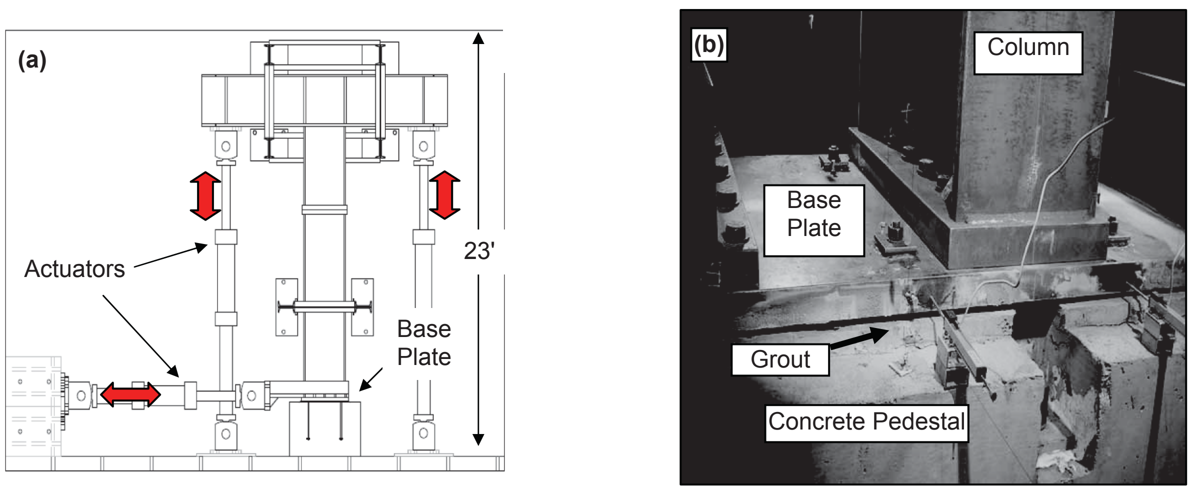

Fig. 2. Test setup: (a) schematic of overall setup; (b) photograph of base plate detail.

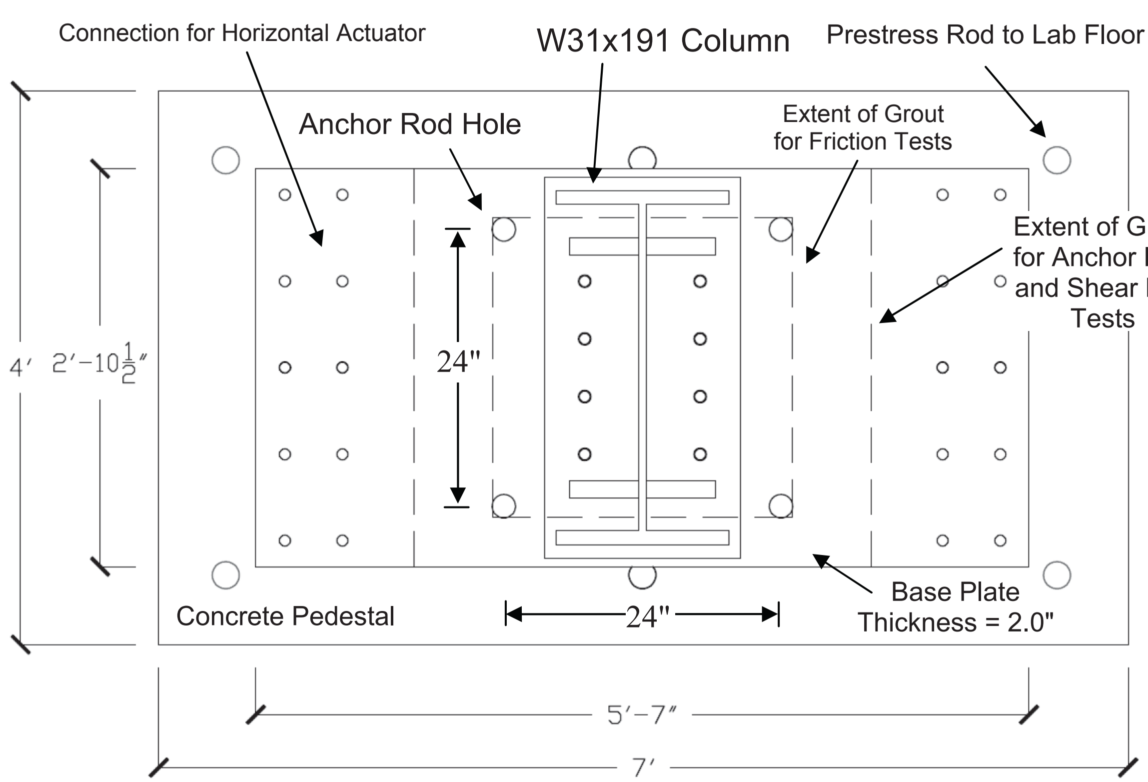

Fig. 3. Plan view of column base plate and footing assembly.

are not readily available for "stiff" mechanisms such as the shear transfer examined in these tests. Thus, the lateral deformation histories applied in this study are based on a number of assumptions as to the demands that may be reasonably expected for each shear transfer mechanism under earthquake loads.

1. **Surface friction tests 1, 2 and 3:** For each test, axial compression was first applied to the base plate, followed by cyclic lateral deformations as per the protocol outlined in Figure 4. This was repeated for three levels of axial load for each specimen. Referring to Table 1, test 1 initially had an imposed axial load of 43 kips, followed by cyclic deformations that ruptured the adhesion bond between the steel plate and the grout. The process was repeated twice more with axial compression load levels of 112 and 261 kips. With a base plate bearing area of about 675 in.^{2}, the three axial load levels imposed compressive bearing stresses of about 64, 166 and 386 psi, which are approximately 2 to 10% of the specified compressive strength of the concrete (4,000 psi). For tests 2 and 3, the same loading process was applied, except that the axial loads were applied in decreasing order, thereby breaking the steel-grout bond at the largest load level.

2. **Anchor rod bearing tests 4 and 5:** For these tests, a tensile axial load was applied and held constant while the cyclic lateral loading (Figure 4) was applied until rod fracture occurred. The axial tensile loads were 40 kips for test 4 and 108 kips for test 5, corresponding to about 31 and 39% of the ultimate tensile capacities of the anchor rods in each specimen, respectively.

3. **Shear key bearing tests 6 and 7:** For both these experiments, a small axial compressive load was applied to prevent lift off of the column base, while lateral shear deformations were applied monotonically until breakout failure was observed. The loading was reversed and applied monotonically until failure in the reverse direction.

Description and Results of Friction Tests 1, 2 and 3

For tests 1 and 2, steel shim stacks were installed to support the base plate during column erection, and test 3 was assembled without shims by suspending the base plate to the desired position via control of the vertical actuators prior to grouting. As shown in Figure 5, different shim stack positioning was used for tests 1 and 2 to ensure that the same region of the reused base plate was not subjected to excessive wear. The shims were thermally cut from ½-in.-thick steel bar stock, each measuring approximately 4 in. by 2 in. in area and stacked two tall for a total thickness of 1 in. The shims were heavily oxidized and had a slightly rough surface. Deposits around the edges from thermal cutting were chipped away, but the shims were not deburred nor surface treated in any other way. The base plate was not surface treated and contained mill scale, typical of as-rolled steel used in standard construction practice. In fact, the AISC *Specification for Structural Steel Buildings* (AISC, 2005c) states that grouted base plates need not be milled. After the base plate was set on the shim stacks, grout was installed by pouring a workable mix through the anchor rod holes into a foam dam beneath the base plate, which provided a grout bearing area of 675 in.^{2} (see Figure 5).

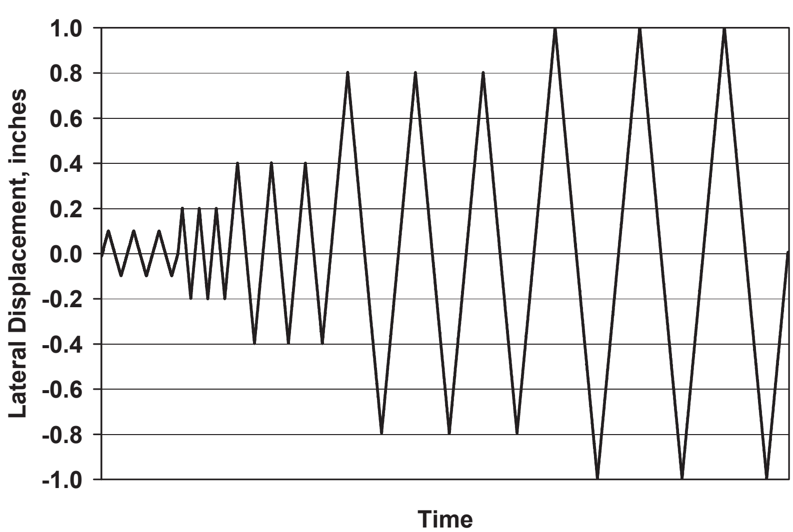

Fig. 4. Lateral loading protocol for surface friction and anchor rod bearing tests (tests 1–5).

A representative lateral load versus deformation response for the friction tests is shown in Figure 6 (shown here for test 3). The response reveals a large initial lateral force corresponding to the rupture of the steel-to-grout adhesive bond, followed by a square-shaped hysteretic response (indicative of Coulomb friction) between the grout and the steel base plate. In addition to mild abrasion marks observed over the entire base plate, moderate scouring damage to the base plate was localized at the locations of the shim stacks. For test 1, only two shim stacks exhibited significant scuffing damage, whereas in test 2, all four shim stacks showed scuffing. Aside from mild spalling of the extreme perimeter of the grout pad, no damage to the grout (other than surface abrasions) was observed. Moreover, no damage to the concrete footing was observed, and the grout retained its bond to the concrete.

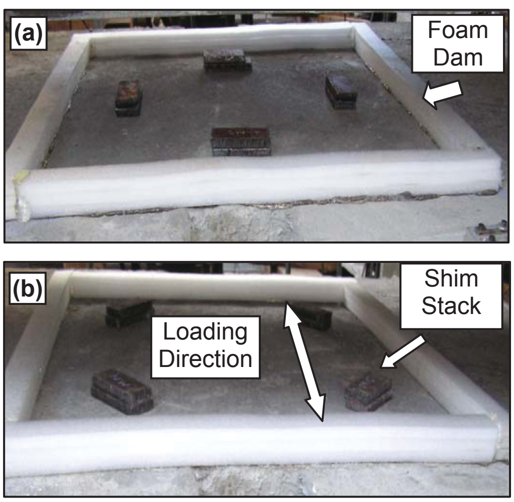

Fig. 5. Shim stack positioning for (a) test 1 and (b) test 2.

Shown in Figure 7 is a plot of the effective coefficient of friction (defined as the ratio of lateral friction force to axial force) versus the cumulative lateral displacement (base plate slip) for each test. As indicated in Figure 7, the effective coefficient of friction varies significantly during the tests. The following observations are made from the tests:

1. For all tests, the initial resistance corresponding to bond breakage of the steel-grout adhesion is about twice as large as the frictional force following bond breakage. This resistance arises from chemical bonding that is distinct from sliding friction resistance. Because bond adhesion may not be present in field conditions over the life of a structure, the shear resistance from adhesion is not considered in the characterization of the coefficient of friction for design.

2. For tests 1 and 2 with shim stacks, the effective coefficient of friction follows a consistent pattern of evolution. After the initial bond breakage, the shear resistance remains relatively constant during the initial loading cycles. Subsequently, the shear resistance increases, which is attributed to the shim stacks gouging into the underside of the base plate (substantiated by the observation that this increase is not evident in test 3 without shims). Because this gouging mechanism occurs only after significant cumulative lateral slip, this increase in the friction may not be available in actual conditions and is therefore neglected for the developing recommendations for design.

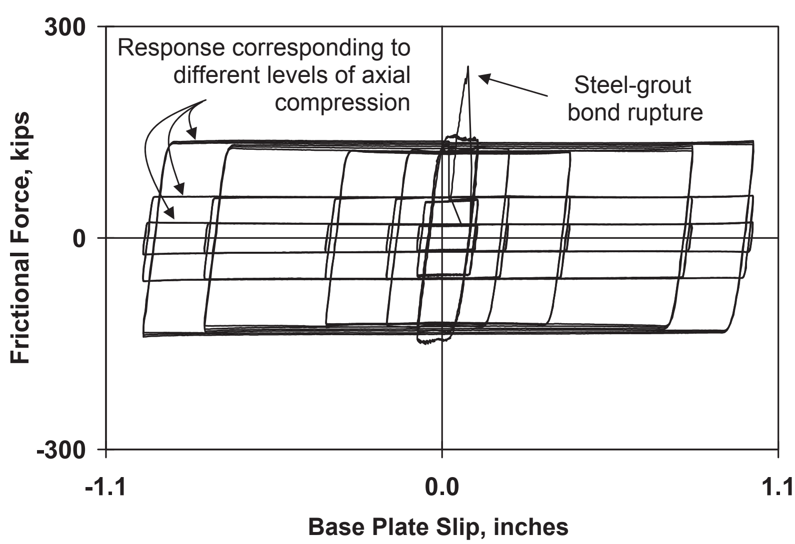

Fig. 6. Representative response plot of the surface friction tests (shown here for test 3).

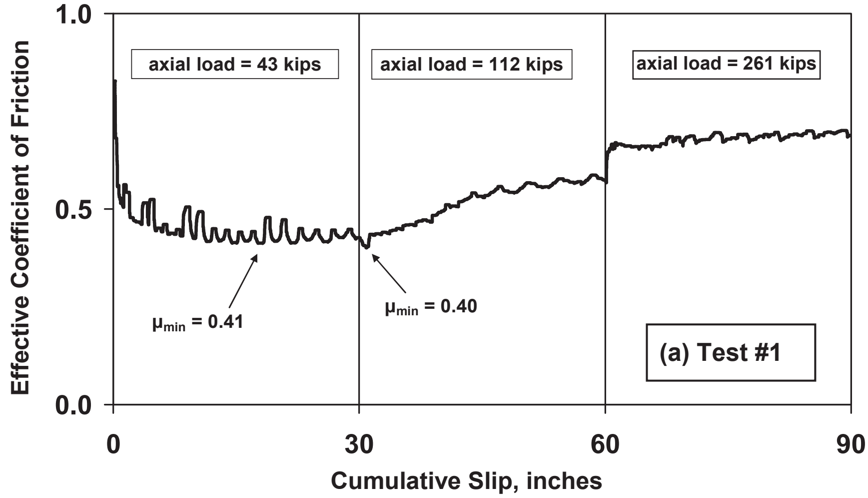

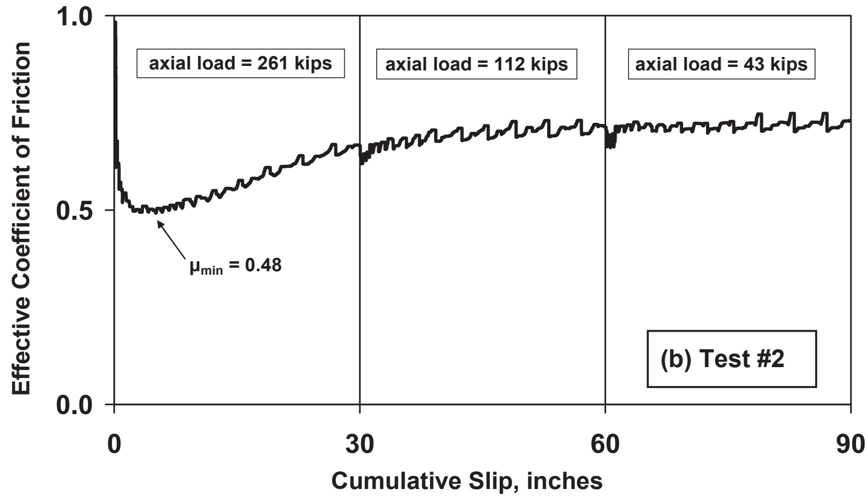

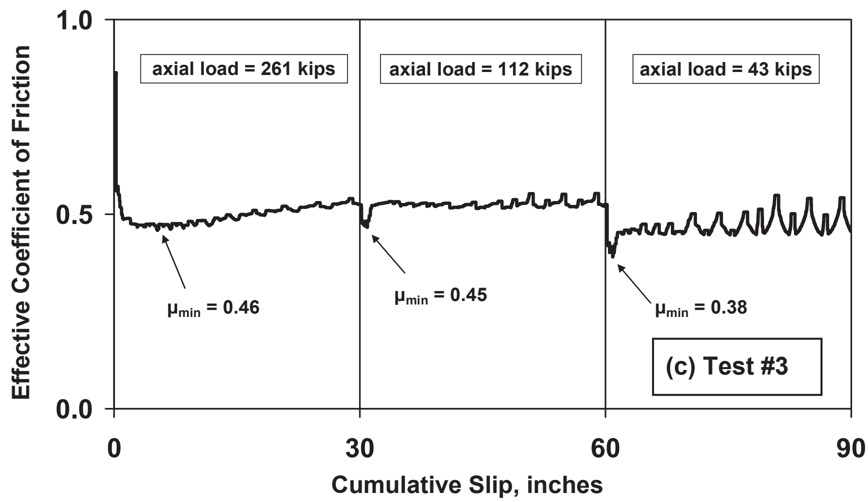

Fig. 7. Response progression of each friction test illustrating the extracted coefficient of friction values used for analysis.

3. Figure 7c shows the evolution of the friction coefficient during test 3. Because this specimen does not include shim stacks, the increase in frictional resistance due to shim gouging is not observed. Slight reductions in the effective coefficient of friction are observed subsequent to each change in axial load level. These occur during cyclic displacement amplitudes of 0.1 in., under which the slip velocity was slower (4.2×10^{-3} in./s) as compared to the remaining cycles (14×10^{-3} in./s). Prior studies of friction between nonmetallic materials on steel (Fenz, 2002) show that frictional resistance decreases as the slip velocity tends to zero.

Based on the preceding observations, the numeric friction coefficients identified in Figure 7 are used to determine suggested design values. These values neglect the effects of steel-grout bonding (chemical adhesion) and shim gouging. Further, assuming that the intent in design is to prevent slip, the selected values are the minimum values that occur early in each loading cycle. As indicated, two data points are extracted from test 1 (see Figure 7a), because the increase in friction corresponding to gouging does not occur until the second axial load level (112 kips). One point is extracted from test 2 (see Figure 7b), because the effects of gouging are significant during the latter cycles of the initial axial load level (261 kips). Three points (see Figure 7c) are extracted from test 3 (which did not include shims). These six points are plotted as a function of axial stress in Figure 8, where there is a clear (statistically significant) linear trend with an effective coefficient of $\mu = 0.46$.

The American Concrete Institute specifies that the coefficient of friction resulting from slip between an as-rolled steel base plate installed against hardened concrete may be taken as 0.40 (ACI 349, 2006). This design value is based on a mean of 0.43 and a standard deviation of 0.09 from 44 base plate surface friction tests by Cook and Klingner (1992). Following this, the AISC *Steel Design Guide 1* (Fisher and Kloiber, 2006) suggests a value of 0.4 for the coefficient of friction. Recent tests by Nagae et al. (2006) report a coefficient of friction value between steel and grout as 0.52. The value determined by the current study (0.46) is comparable to these previously reported values. The surface condition of the steel base plate (i.e. steel with or without mill scale), grout properties and the level of normal stress may affect the friction response. As shown in Figure 8, while the coefficient of friction was constant over the range of normal stresses, the maximum normal stress applied in these tests was about 390 psi. A series of friction tests between steel and concrete by Baltay and Gjelsvik (1990) indicates that the coefficient of friction for steel with mill scale (such as in the current investigation) is lower than that for a machined (i.e., polished) surface for bearing stress levels below 10,000 psi. This is attributed to the high hardness of the mill scale (relative to steel), because the hard mill scale is less easily penetrated by the concrete/grout particles at lower bearing stress levels, resulting in a lower coefficient of friction. Nevertheless, a value of 0.46 for the coefficient of friction between a steel base plate and grout pad (with or without steel shim stacks) is conservatively recommended based on experimental data from this study. Sometimes, leveling nuts may be used to level the plate instead of shim-stacks. While it is difficult to anticipate the response of these details (because they have not been tested), one may speculate that their responses will be similar to those of the specimens with the shim stacks.

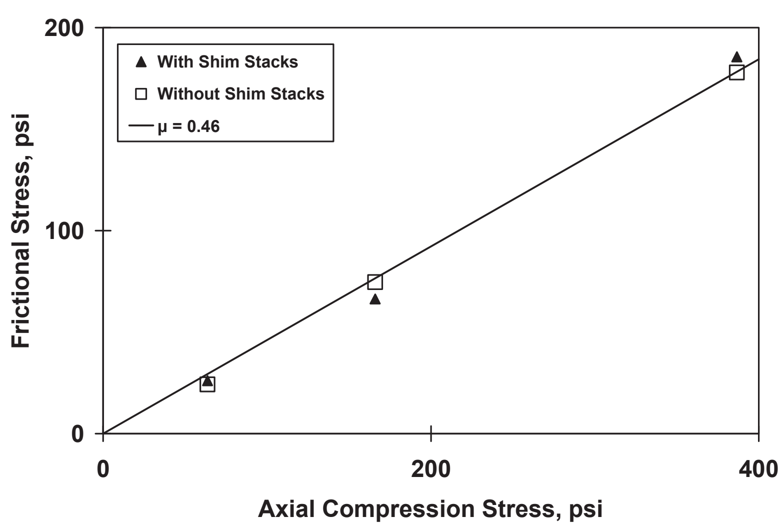

Fig. 8. Scatter plot used to determine the coefficient of friction.

Description and Results of Anchor Rod Bearing Tests 4 and 5

Tests 4 and 5 were designed to investigate shear transfer capacity through anchor rod bearing against the base plate under imposed tension axial loads and shear (such as would be observed during uplift due to structural overturning moments or brace tensile forces). Test 4 had four ¾-in.-diameter rods, and test 5 had four 1¼-in.-diameter rods. All rods were ASTM F1554 Grade 55 steel and were installed such that the rod threads extended approximately 2 in. below the surface of the concrete pedestal to ensure that failure occurred in the threaded region. The ¾-in.-diameter rods had a measured shank diameter of 0.75 in. and measured strengths of F_y = 66.8 ksi and F_u = 96.4 ksi. The 1¼-in. rods had a measured shank diameter of 1.25 in. and measured strengths of F_y = 54.4 ksi and F_u = 75.0 ksi. The ultimate shear strength is assumed to be 0.6 times the tensile strength. The concrete footings and anchor rods were designed to ensure failure of the anchor rod itself, rather than anchor rod pullout or concrete breakout. Based on compression tests of cylinder samples, the grout had measured compressive strengths of 6,100 psi (test 4) and 7,200 psi (test 5); the concrete footings had measured compressive strengths of about 4,600 psi.

In accordance with the AISC *Steel Design Guide 1* (Fisher and Kloiber, 2006), the base plate has oversized anchor rod holes of 2¹⁄₁₆-in.-diameter to provide tolerances for 1¼-in.-diameter anchor rods used in test 5. Because the same base plate was used for test 4, these 2¹⁄₁₆-in. holes were larger than the recommended size for ¾-in. anchor rods. To help prevent slip and ensure distribution of shear to all anchor rods, plate washers were fillet welded to the base plate (see Figure 2b). Although this may not be common practice, it

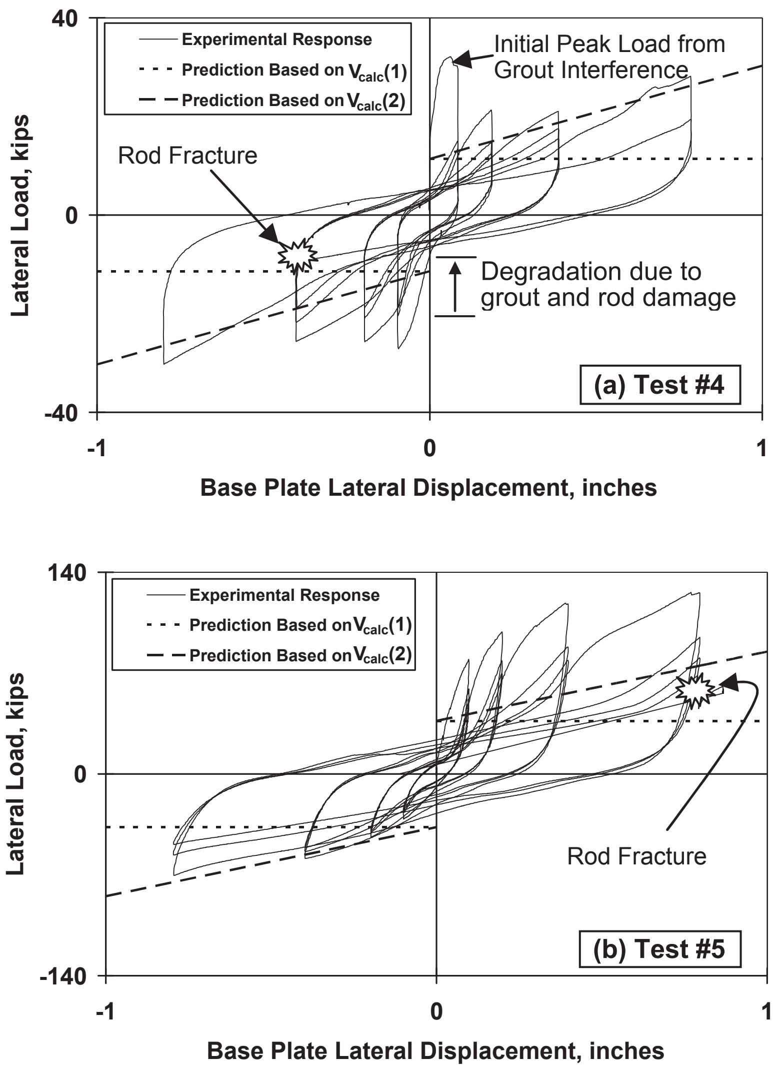

Fig. 9. Experimental response plots of the anchor rod bearing tests.

is recommended (Fisher and Kloiber, 2006) for situations where anchor rod bearing is the designated mechanism for shear transfer. For test 4, these washers measure 2.5 in. × 2.5 in. × ¼ in. with an internal hole diameter of 0.8 in. (rod diameter plus 1⁄16 in.), and for test 5, the washers measure 3.5 in. × 3.5 in. × ½ in. with an internal hole diameter of 1.3 in. Additional washers were placed (unwelded) on top of the welded plate washers to prevent dishing of the welded plate washers due to the large tension forces in the rods. Nuts were installed snug tight with no significant level of prestress. A stiff grout mix was placed on the concrete pedestal, and the base plate was lowered to the desired position via control of the vertical actuators. The grout was compacted to a thickness of 1¼ in. for test 4 and a thickness of 1 in. for test 5, and excess grout was removed from the anchor rod holes prior to curing.

Referring to Table 1, axial tension of 40 kips (equal to about 31% of the measured anchor rod capacity) was applied in test 4, and axial tension of 108 kips (equal to about 39% of the anchor rod capacity) was applied in test 5. This axial load was held constant while cyclic shear deformations (Figure 4) were applied.

In general, the anchor rod tests 4 and 5 followed a similar progression of events. The initial tensile uplift loading ruptured the chemical adhesion between the steel base plate and the grout pad, creating a small gap between the base plate and grout. During subsequent cyclic shear loading, the gap enlarged due to plastic elongation (flow) of the anchor rods, and these anchor rods were cycled in shear under constant axial load. By the end of the test, the base plate displaced vertically approximately 0.4 in. for test 4 and 0.6 in. for test 5. Shown in Figure 9 are plots of lateral load versus lateral base plate displacement for both tests, where each test was concluded when one anchor rod fractured. Table 1 summarizes the maximum lateral load recorded in the positive and negative loading cycles.

Inspections made after completion of the tests revealed extensive damage to the grout, especially in the vicinity of the anchor rods. No damage was observed to the concrete footing in test 4, where one ¾-in. anchor rod fractured approximately ¼ in. above the footing surface (i.e., within the grout pad, illustrated in Figure 10). Slight damage to the concrete footing was observed in test 5, including local spalling cones around the perimeter of each rod, generally 2 to 4 in. in diameter and about 1 in. deep. In test 5, one anchor rod fractured about 1 in. below the surface of the concrete, and the other rods showed significant residual deformations up to about 1 in. below the surface of the damaged concrete.

The following explanation of the response is based on visual observations during testing, the measured load-deformation response (Figure 9), post-test inspection of the deformed anchor rods and damaged grout (Figure 10) as idealized models of the anchor rod behavior (Figure 1c):

1. The large initial lateral resistance in test 4 is attributed to grout that was not completely removed from the four base plate anchor rod holes. The highly confined grout stubs (rising approximately 0.75 in. within the anchor rod holes) constrained the movement of the anchor rods and the base plate, thus developing a relatively high initial load. This strength dropped quickly when the grout crushed. This phenomenon was not observed in test 5.

2. Apart from the early peak observed in test 4, the lack of symmetry in the response and the larger resistances observed at certain points in the loading history may be attributed to the impingement of the lower edge of the base plate on the anchor rods. This is observed in the lower-left quadrant in test 4 (Figure 9a) and the upper-right quadrant in test 5 (Figure 9b). Referring to Figure 1c and Figure 10, this impingement reduces the effective bending length of the anchor rod and dramatically stiffens the shear transfer. At this point, the affected anchor rod begins to transfer force in direct shear through local bearing against the bottom of the base plate and grout, as opposed to shear and bending. Upon load reversal, the force transfer becomes quite flexible until the opposing hole edge impacts the anchor rod, leading to extreme pinching behavior. In rods where this bearing occurs, the grout becomes extensively damaged due to the high shear transfer force.

3. Where bearing of the plate washers (rather than the base plate) on the anchor rod occurs, the resistance tends to increase gradually with increasing deflections and degrade under reversed cyclic loading. The strength increase under increasing deformations is due to tension stiffening, such that the horizontal component of the anchor rod tensile force resists the applied shear. The degradation is associated with plastic deformations of

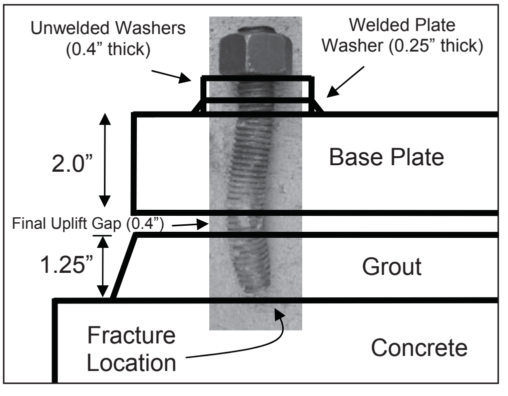

Fig. 10. Deformed anchor rod from test 4 superimposed on base plate assembly detail.

the rods and damage to the grout pad, which tends to increase the bending length of the anchor rods and decreases their lateral force resistance due to bending and tension stiffening.

The AISC *Steel Design Guide 1* includes a procedure wherein the anchor rod strength is calculated considering the interaction of axial, shear and flexural stresses. The anchor rod is assumed to deform in double (reverse) curvature over a length corresponding to the distance between the top of the grout pad and the center of the welded plate washer (Figure 1c). The strength limit state is controlled by a critical combination of the tensile stress (due to axial load and bending) and shear stress. The combined stress limit state is evaluated according to Equation C-J3-5a from the AISC *Specification* (AISC, 2005c):

$$\left(\frac{f_t}{\phi F_{nt}}\right)^2 + \left(\frac{f_v}{\phi F_{nv}}\right)^2 = 1 \tag{1}$$

where

F_{nt} = ultimate tensile strength of anchor rod, ksi

F_{nv} = ultimate shear strength of anchor rod, ksi

f_t = applied tensile stress, ksi

f_v = applied shear stress, ksi (MPa)

The applied tensile stress arises due to a combination of axial force and flexure. The shear and tensile stresses in each rod are calculated as:

$$f_v = \frac{V_{rod}}{A} \tag{2}$$

$$f_t = \frac{P_{rod}}{A} + \frac{M_{rod}}{Z} \tag{3}$$

where

V_{rod} = applied shear force in each anchor rod (typically total force in connection divided by number of rods), kips

P_{rod} = applied axial force in each anchor rod, kips

A = cross-sectional area of anchor rod, in.^{2}

Z = plastic section modulus of rod cross-section, in.^{3}

M_{rod} = klV_{rod} = moment in rod, kip-in.

k = effective length factor for rod (or level arm factor, such that $k = 0.5$ for a rod bending in double curvature with complete fixity at both ends, and $k = 1$ for a cantilever deformation mode)

The AISC *Steel Design Guide 1* recommends a value of k equal to 0.5 and l as the distance between the top of the grout to the center of the welded plate washer (see Figure 1c). This distance l equals 2.125 in. for test 4 and 2.25 in. for test 5. Given these values and the axial load, P_{rod}, Equations 2 and 3 can be substituted into Equation 1 to determine the shear capacity V_{rod}. For calculating stresses on the net section of the threaded rods, AISC *Steel Design Guide 1* assumes the anchor tensile stress area to be of 75% the nominal (unthreaded) rod area. Alternatively, the net tensile area is more accurately calculated based on the number of threads per inch and the measured unthreaded diameter (Table 7-18 in the 2005 AISC *Steel Construction Manual*). Based on Equations 1, 2 and 3, and using the measured rod material properties and geometries, the shear strength of the four-rod connections for tests 4 and 5 are calculated as 11.4 kips and 36.9 kips, respectively. These predicted strengths are overlaid on the plots in Figure 9 and are listed as the $V_{calc}(1)$ values for tests 4 and 5 in Table 1. From a mechanics standpoint, the relationship implied by Equation 3 (i.e., the superposition of plastic stresses due to flexure and axial load) is inadmissible. However, Hill and Siebel (1951) demonstrate that for circular cross-sections, a closed-form solution for the plastic interaction diagram cannot be obtained. Thus, Equation 3 represents a linear fit to this plastic interaction relationship that is accurate for both $P_{rod} = 0$ and $M_{rod} = 0$. Experimental data indicate that the error is modest between these extreme points.

As the base plate displaces laterally and the anchor rods tilt, lateral resistance is increased by the horizontal component of the tensile force in the anchor rods. Based on a small-angle assumption, the additional horizontal contribution of shear resistance, $V_{T-\Delta}$, may be expressed as:

$$V_{T-\Delta} = T\left(\frac{\Delta}{l}\right) \tag{4}$$

where

T = vertical tensile force in anchor rods, kips

Δ = lateral displacement (slip) of base plate, in.

l = length over which anchor rod deforms, in.

Based on the applied tensile forces (40 and 108 kips in tests 4 and 5, respectively) and assuming that the deformation length, l, is the same as the bending length used previously (base plate thickness plus one-half of the welded plate washer thickness), the additional shear resistance provided by $V_{T-\Delta}$ is indicated by the sloped lines in Figure 9. At the maximum imposed displacement of $\Delta = 0.8$ in., the resulting shear resistance is 26.5 kips for test 4 and 75.3 kips for test 5 [reported as $V_{calc}(2)$ in Table 1].

Referring to Figure 9 and Table 1, the mechanism provided by combined anchor rod bending (Equations 1, 2 and 3) and tension stiffening (Equation 4) gives a reasonable estimate of the shear transfer strength [i.e., $V_{calc}(2)$] in Table 1. These mechanisms assume reverse curvature bending over a free bending length equal to the combined thickness of the column base plate and one-half thickness of the welded plate washer. Direct bearing between the anchor rod and either the bottom of the base plate or grout installed inside the oversized base plate holes can significantly increase the resistance. However, these bearing mechanisms are highly variable because they depend on the construction tolerances and placement of the anchor rods and grout, and they occur at large deformations.

For design where one does not generally expect to see significant base plate slip, the approach currently outlined by the AISC *Steel Design Guide 1* (Fisher and Kloiber, 2006) provides a reasonable (albeit conservative) measure of the strength associated with shear transfer through anchor rod bending. While damage to the grout is likely to occur under cyclic loading, it is assumed the resulting negative effects of the increase in anchor rod bearing length are counteracted by tension stiffening effects and base plate impingement, which occur under larger deformations.

Description and Results of Shear Key Bearing Tests 6 and 7

Tests 6 and 7 investigated shear transfer through bearing of a shear key embedded in the concrete footing (Figure 1d). Several failure modes may contribute to shear key failure, including concrete bearing failure, edge breakout failure of the concrete foundation, shear key yielding or fracture of the shear key welds, or flexural yielding in the base plate. In this study, the shear key was fabricated from heavy plates and intentionally designed to remain elastic, with the weakest failure mode being breakout failure in the edge of the concrete footing. Shown in Figure 11a is a photograph of the I-shaped shear key, which measured 6 in. wide and 7.5 in. deep (parallel to the base plate) and was welded to the underside of the base plate. For test 6, the shear key was 7 in. long, and after this test, the shear key was cut to 4.5 in. deep for test 7. Grout pockets in the concrete footing measured 9 in. × 9 in. in plan and 7 in. deep for test 6 and 4.0 in. deep for test 7. Grout was installed by pouring a highly flowable mix through grout holes in the base plate. Steel shims measuring 1.5 in. thick were installed below the base plate, resulting in a shear key embedment depth (below the surface of the concrete) of 5.5 in. for test 6 and 3.0 in. for test 7. The distance from the shear key bearing surface to the edge of the concrete pedestal was 20.25 in. (see Figure 11b). The anticipated concrete blowout area (i.e., failure region) of the footing was free of any reinforcement or other obstructions (with the exception of the anchor rods), to ensure that the obtained failure represented plain (i.e., unreinforced) concrete capacity only. The ¾-in. anchor rods, used in both tests, were not connected to the base plate but were included to simulate concrete confinement offered by the rods.

The specimens in tests 6 and 7 were loaded to failure in monotonic shear in the forward and reverse loading directions. To prevent liftoff of the plate during testing, a small compressive axial load (approximately 14 kips for test 6; 15.4 kips for test 7) was applied simultaneously with the lateral load. The measured lateral forces were separated into the component of force carried by the shear key and by friction, assuming a friction coefficient of 0.46 multiplied by the applied compressive forces.

Load-deformation plots for both the shear key tests are shown in Figure 12, where two curves are plotted for each test for the forward and reverse loading directions. Because the failure was confined to the concrete footing, the damage and failure modes in each direction were independent of each other, such that data collected for the reversed loading direction are assumed to reflect undamaged initial conditions. This independence is supported by visual observations and the load-deformation plots, which are similar in the two directions.

Qualitatively, both tests showed a similar evolution of damage. After the initial elastic increase in load, an initial sudden load drop was observed. This was accompanied by the formation of a long vertical crack running down the center of the free edge of the concrete footing (see Figure 13a), corresponding to flexural cracking of the unreinforced pedestal. As loading progressed, the load began to steadily increase, while the central crack in the footing opened further (see Figure 13b). After this, new shear cracks were observed, propagating outward from the edge of the shear key at approximately 60° to the loading direction (see Figure 13c), resulting in the drop in strength at the second peak load observed in the force-deformation plots. This behavior is somewhat similar to shear cracks in concrete beams (see MacGregor and Wight, 2004). Finally, continued propagation of the shear cracks led to edge breakout failure of the footing. This failure occurred at small lateral displacements (on the order of 0.2 in.) indicating the high stiffness of the failure mechanism. The post-test condition of the footing of test 6 is shown in Figure 14. The peak final loads from both the tests are summarized in Table 1.

Two methods are considered to calculate the strength corresponding to the concrete blowout failure of the concrete footing. One of these methods, commonly referred to as the 45° cone method, is prescribed by ACI 349-06 for the concrete shear capacity of embedded shear lugs and is featured in the AISC *Steel Design Guide 1* (Fisher and Kloiber, 2006). As per an adaptation of this method for footings, the concrete strength capacity is given as:

$$V_n^{45} = \left(4\sqrt{f_c'}\right) A_{45}, \text{ lb} \tag{5}$$

where

f_c' = concrete compressive strength, psi

A_{45} = effective stress area, in.^{2}

The effective stress area is defined by projecting 45° planes from the bearing edges of the shear key to the free edge of the concrete (see Figure 11b, θ = 45°). The bearing area of the shear lug is excluded from this projected area. The 45° cone method assumes a uniform tensile strength of $4\sqrt{f_c'}$ (in psi) acting on the effective stress area.

The second method for calculating the concrete footing strength is based on the concrete capacity design (CCD)

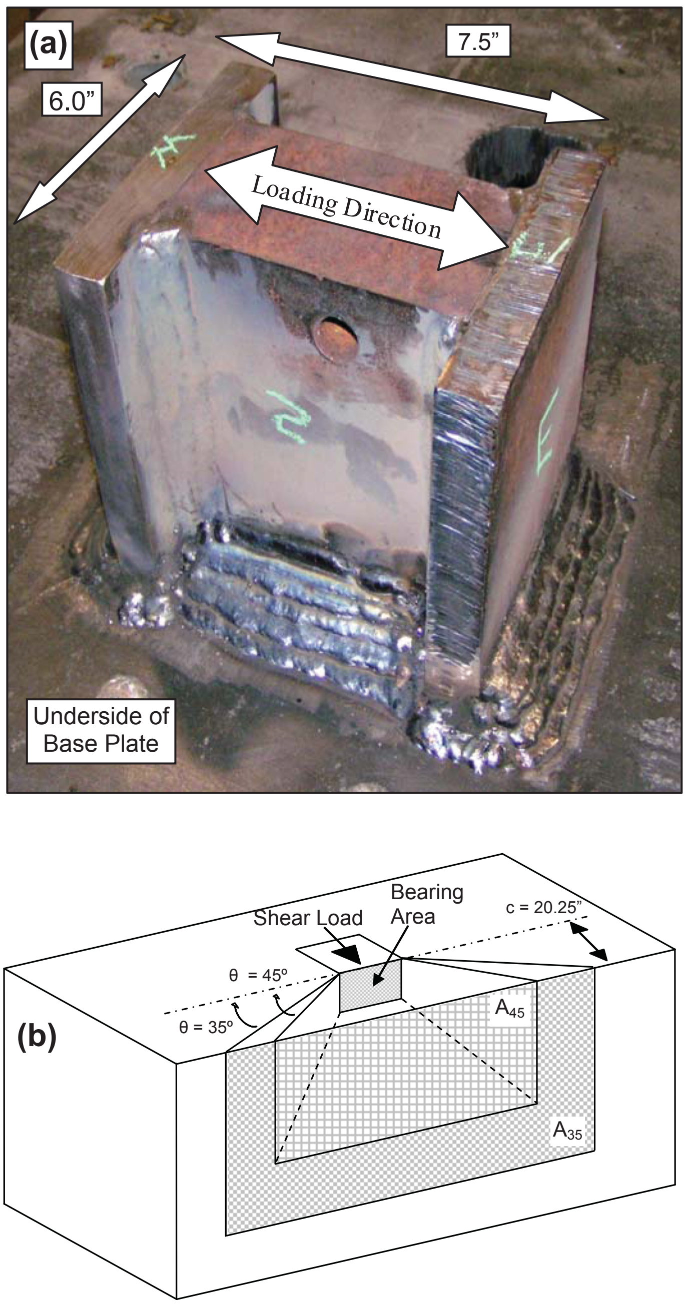

Fig. 11. (a) Photograph of the shear key and (b) schematic illustrating the effective stress area assumed by the 45° cone method (A_{45}) and the CCD method (A_{35}).

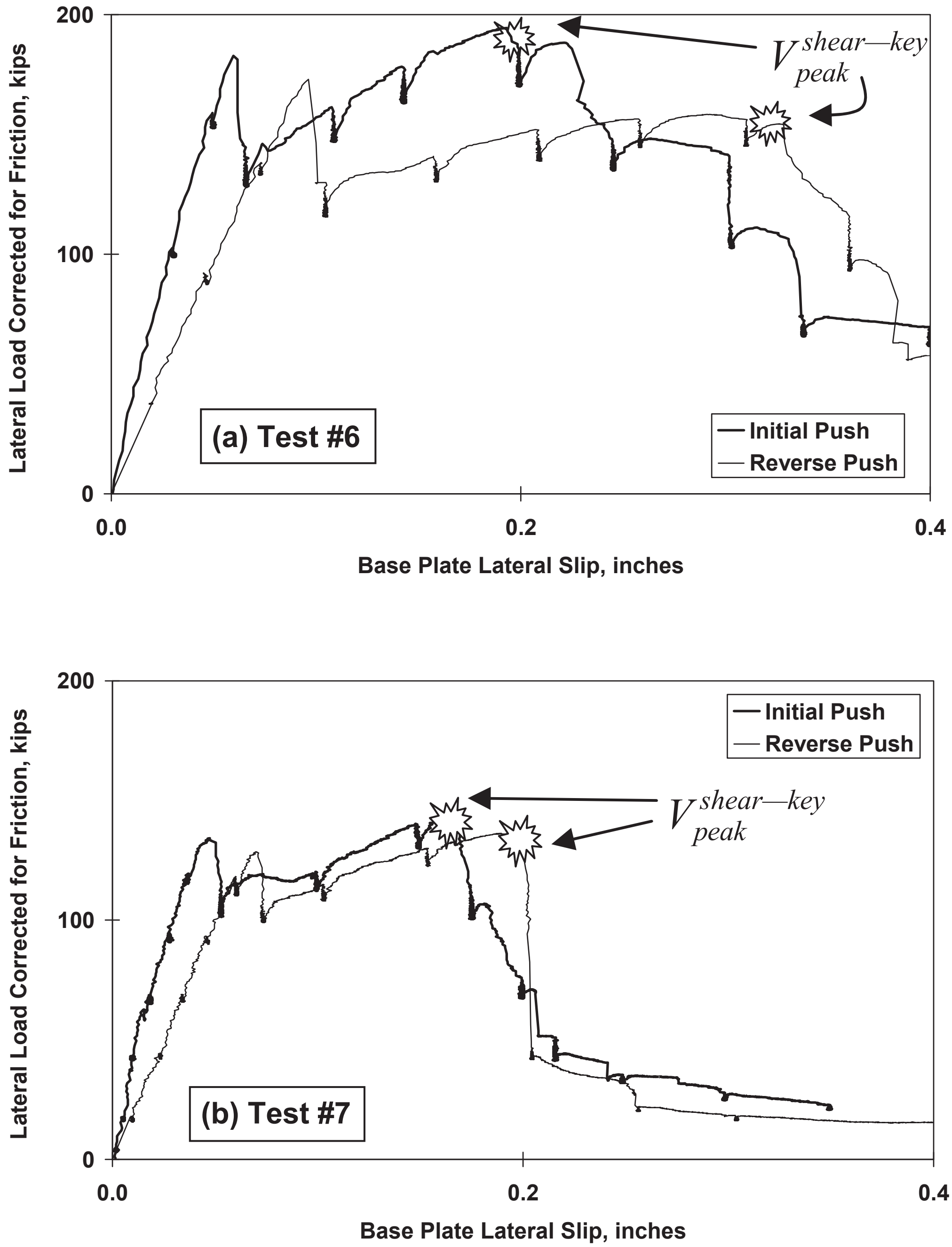

Fig. 12. Experimental response plots of the shear key bearing tests.

method, which has been adapted by ACI 318-08 for anchorages in concrete under tension or shear loading. As per this method, the strength is determined as:

$$V_n^{CCD} = \frac{1}{\sqrt{c}}\left(\frac{40}{9}\sqrt{f_c'}\right)A_{35}\text{, lb} \tag{6}$$

where

A_{35} = projected area, in.^{2}

c = edge distance, in.

The projected area is similar to A_{45} described earlier, except that the planes are projected at approximately 35° to the free edge (≈ 55° to the loading direction; see Figure 11b, $\theta = 35°$). In contrast to Equation 5, the CCD method assumes that the tensile stress acting on this projected area also depends on the edge distance c between the shear key and the free edge of the concrete. A detailed derivation of Equation 6, indicating its adaptation from the CCD method proposed originally by Fuchs et al. (1995) is presented in Gomez et al. (2009).

The main underlying difference between these two strength models is associated with the size effect in concrete derived from fracture mechanics theory (see Bažant, 1984). As per Equation 5 for the 45° cone method, the concrete failure strength is directly proportional to the projected effective stress area. While this is often true for smaller geometries, where the specimen dimension is approximately 10 to 20 times the aggregate size (Bažant, 1984), failure in larger specimens is governed by fracture mechanics, because the initiation of cracking in the concrete, rather than the development of a uniform stress over a failure surface, controls the failure strength. Research by Bažant (1984) and others (Fuchs et al., 1995) has shown that this size effect may be successfully incorporated by expressing the failure stress as a function of the specimen size (conveniently characterized here by the embedment free-edge distance, c). Thus, for larger specimens, the failure stress is lower as compared to that for small specimens.

It is useful to compare the effective failure stress areas implied by the two methods. The area of the 45° cone method is based on physical interpretation, because this method assumes that the concrete tensile strength is activated over this area. Conversely, in the fracture-based expression for the CCD method, it is assumed that failure occurs due to the initiation of cracking over a small region in the vicinity of the shear key. Once crack initiation occurs, the load drops steadily as the shear cracks grow and the failure region expands. Thus, the area A_{35} in Equation 6 does not bear any physical significance as to the final failure surface, but, rather, may be interpreted as a basis for the characterization of the nominal stress required to produce fracture.

Along with the measured strengths, Table 1 summarizes the calculated strengths using the standard 45° and CCD methods, reported as $V_{calc}(1)$ and $V_{calc}(2)$, respectively. The predicted strengths are based on the average 28-day concrete strengths measured from cylinders collected for each of the footings (4,650 psi for test 6 and 5,030 psi for test 7).

From the summary data in Table 1, it is clear that the CCD method is much more accurate than the 45° cone method for calculating the concrete blowout strength. Whereas the 45° cone method (as prescribed by ACI 349 and recommended in the AISC *Steel Design Guide 1*) overestimates the measured strengths by about a factor of 2, the mean ratio of the test-to-calculated strengths from the CCD method is $V_{peak}^{shear-key} / V_n^{CCD} = 1.07$ with a coefficient of variation (COV) of 0.19. The observed failure surface, which is approximately 30° to the free edge (see Figures 13 and 14), is also closer to the nominal fracture surface of the CCD

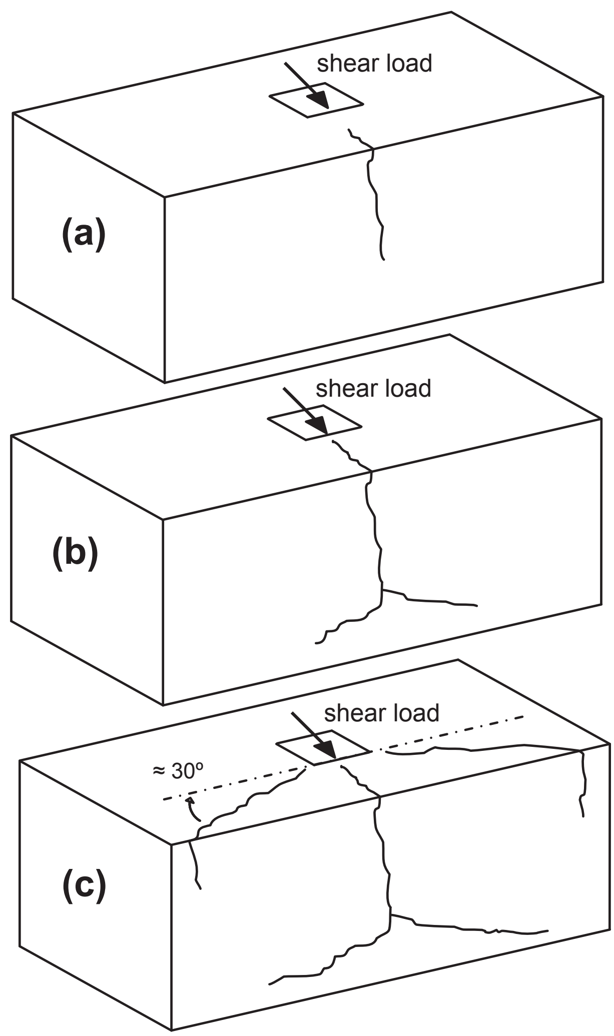

Fig. 13. Damage progression for shear key test 6: (a) 0.066-in. slip; (b) 0.144-in. slip; (c) 0.246-in. slip.

method. Comparing results between tests 6 and 7, the CCD method is less accurate for the deeper 5.5-in. shear key (mean $V_{peak}^{shear-key} \big/ V_n^{CCD} = 1.22$) as compared to the 3.0-in. deep shear key (mean $V_{peak}^{shear-key} \big/ V_n^{CCD} = 0.92$). The effective stress area, A_{35}, is nearly identical for the two shear key lengths (less than 1% difference), whereas the measured strength of test 6 (longer shear key) is about 26% greater than test 5. This suggests that the longer shear key is stronger on a unit basis, as compared to the shorter one, which may be attributed to the larger local bearing stresses associated with the smaller shear key embedment length. As evidenced in numerical studies (Ožbolt et al., 2007), a higher bearing stress increases the likelihood of early crack initiation and failure.

Based on the preceding observations, the CCD method provides a relatively accurate estimate of strength for embedments with large free-edge clear distances (i.e., large concrete foundations), where the strength is controlled by fracture initiation. Although not tested as part of this study, it is anticipated that for small edge distances, where the strength is governed by development of the concrete tensile strength over the failure area, the CCD method may provide unconservative results. Thus, it is recommended that the reliable strength of concrete blowout due to shear key bearing be calculated as the minimum of the two estimates, such that for smaller edge distances, the 45° cone method will govern, while for larger edge distances, the CCD method will govern. Comparing the two equations, the limiting edge distance (i.e., for which both methods produce a similar estimate) is fairly small—on the order of 6 in. (or about 5 to 10 times the aggregate size, which is in approximate agreement with the fracture mechanics theory proposed by Bažant, 1984). The size effect in concrete is assumed to diminish in the presence of steel reinforcement, which increases the ductility of the concrete pedestal, thereby providing the opportunity for the redistribution of stresses over a larger volume of material. However, the beneficial effect of reinforcement is difficult to quantify in the absence of additional testing. In some cases, the shear key may be positioned close to a corner, or the foundation may not be deep enough to develop the full projected effective area. Methods and schematics for calculating these areas are provided in Gomez et al. (2009). For very large free-edge clear distances, the shear strength may be governed by bearing failure of the concrete (see Hawkins, 1968), in which a wedge-like failure surface may develop at the top surface of the concrete.

Fig. 14. Edge breakout failure surface of concrete footing (test 6).

SUMMARY AND CONCLUSIONS

This paper presents findings from seven full-scale tests of column base connections subjected to a combination of shear and axial loads. The main focus of the paper is to examine three shear transfer mechanisms that are commonly used in the design of exposed column base plate connections. These mechanisms, featured in the AISC *Steel Design Guide 1—Base Plate and Anchor Rod Design* (Fisher and Kloiber, 2006), include surface friction, anchor rod bearing and shear key bearing. Based on the reported test data and previously published literature, modifications and suggestions are proposed to improve the accuracy for predicting the strength of these three mechanisms.

Three tests of bearing surface friction examined the friction coefficient between steel and grout under bearing stresses ranging from about 60 to 390 psi and in base plate details with and without shim stacks. The tests demonstrated that for details without steel shims, the friction coefficient is fairly insensitive to either cyclic loading or the bearing stress. Tests with shim plates showed that under cyclic loading, the frictional resistance increases due to local gouging between the shim stack and base plate. Based on these tests, a coefficient of friction value of 0.46 is recommended for use in design. This value is comparable to previous tests and the design value of 0.40 provided in ACI 349-06 for as-rolled base plates installed against concrete.

Two tests investigated the shear resistance of anchor rods under a combination of imposed axial tensile (uplift) loads and cyclic shear loading at the base plate. The connection detail included welded plate washers to minimize slip and ensure equitable force distribution amongst all four anchor rods. Two rod sizes, ¾-in.- and 1¼-in.-diameters (both ASTM F1554 Grade 55 steel) were tested. Based on a detailed analysis of data, the current approach prescribed by the AISC *Steel Design Guide 1* (Fisher and Kloiber, 2006) is determined to provide a reasonably conservative strength estimate for design. As per this approach, the anchor rods are assumed to bend in reverse curvature over a distance between the top of the grout pad and the center of the welded plate washer. Thus, the effective length is equal to the thickness of the base plate plus half the thickness of the plate washer. The tests further confirmed that the shear resistance will increase under displacement (slip) of the base plate.

However, it is not recommended to rely on this increased resistance for the nominal strength check.

Two tests examined the use of shear keys to quantify the strength associated with concrete footing failure by breakout of the free edge. The test data indicate that the 45° cone method, as currently prescribed by ACI 349-06 and recommended by the AISC *Steel Design Guide 1*, is significantly unconservative for large concrete foundations due to size effects in concrete, where failure is controlled by fracture initiation. The fracture mechanics–based concrete capacity design (CCD) method provides a more accurate estimate of concrete blowout strength and is therefore recommended for design. The 45° cone method is expected to govern when the concrete footing is small (i.e., the edge distance is on the order of 10 times the aggregate size), although such configurations are not usually encountered in design.

It is important to note that owing to the expense associated with large-scale testing, the data presented in this paper do not include replicate data sets for statistical analysis. Thus, appropriate resistance factors (ϕ factors) should be developed through examination of previous standards, specifications and similar test data. Finally, in field details, several of the mechanisms discussed in the study may be simultaneously active (e.g., friction and anchor rod bearing), and while it is assumed that the component strengths can be combined, this has not been confirmed experimentally. An examination of the interactive effects of these various mechanisms is recommended for future study.

ACKNOWLEDGMENTS

This project was funded by the American Institute of Steel Construction (AISC) and the National Science Foundation (NSF; Grant Number NSF-CMMI 0421492). Trans Bay Steel Corporation of Fairfield, California, and PDM Steel Service Centers Inc. of Stockton, California, generously donated and fabricated steel materials for this research, and their donations are gratefully acknowledged. The authors also thank Mr. Tom Schlafly and Mr. Kurt Gustafson of AISC and Mr. Rick Drake of Fluor Corporation, who provided valuable advice and review of the testing plans. The large-scale experiments described in this report were conducted at the Network for Earthquake Engineering Simulation (NEES) equipment site at the University of California at Berkeley in Richmond, California. The authors would also acknowledge the NEES site staff (Don Clyde, Shakhzod Takhirov, Nathaniel Knight, David MacLam, Donald Patterson and Jose Robles) for assistance during all phases of planning and testing, and Jorge Camacho and Marshall Roberts from the University of California at Davis and Chris Smith of Stanford University for assisting with the testing. The findings and opinions of this report are those of the authors and do not necessarily represent those of the major sponsors (i.e., AISC or NSF).

SYMBOLS

A	Effective cross-sectional area of the anchor rod, in.^{2}
A_{35}, A_{45}	Effective stress area defined by projecting 35° and 45° planes from the bearing edges of the shear key to the free edge of the concrete, respectively, not including the shear key bearing area, in.^{2}
COV	Coefficient of variation
F_{nt}, F_{nv}	Ultimate tensile and shear strengths of the anchor rod, respectively, ksi
F_y, F_u	Measured yield and ultimate tensile strengths of the anchor rod, respectively, ksi
M_{rod}	Maximum bending moment in each anchor rod, kip-in.
P_{rod}	Axial force in each anchor rod, kips
T	Vertical tensile force in the anchor rods, kips
$V_{calc}(1)$, $V_{calc}(2)$	Calculated strength based on alternate prediction methods, kips
$V_{measured}$	Ultimate peak shear resistance observed from the large scale tests, kips
V_{rod}	Shear force in each anchor rod, kips
$V_{T\text{-}\Delta}$	Additional horizontal contribution of anchor rod shear resistance, kips
V_n^{45}, V_n^{CCD}	Strength estimate of concrete breakout based on the 45° cone method and the concrete capacity design (CCD) method, respectively, lb
$V_{peak}^{shear-key}$	Ultimate peak shear resistance observed for the shear key tests corrected for friction, lb
Z	Plastic section modulus of the anchor rod cross-section, in.^{3}
c	Distance from the bearing surface of the shear key to the free edge of the concrete foundation, in.
f_c'	Compressive strength of concrete, ksi
f_t, f_v	Applied tensile and shear stresses, respectively, ksi
k	Effective length factor of the anchor rod (i.e., lever arm factor)
l	Effective bending length of anchor rod; length over which rod deforms, in.
Δ	Lateral displacement (slip) of the base plate, in.

θ Angle from the plane parallel with bearing surface of the shear key to the concrete failure surface, °

μ Coefficient of friction

μ_{min} Minimum coefficient of friction value extracted from the friction tests for the development of the design coefficient of friction value

ϕ Resistance factor

REFERENCES

ACI Committee 318 (2008), *Building Code Requirements for Structural Concrete and Commentary*, ACI 318-08/ ACI 318R-08, American Concrete Institute, Farmington Hills, MI.

ACI Committee 349 (2006), *Code Requirements for Nuclear Safety Related Concrete Structures and Commentary*, ACI 349-06/ACI 349R-06, American Concrete Institute, Farmington Hills, MI.

Adihardjo, R. and Soltis, L. (1979), "Combined Shear and Tension on Grouted Base Details," *Engineering Journal*, AISC, Vol. 16, No. 1, pp. 23–26.

AISC (2005a), *Steel Construction Manual*, 13th ed., American Institute of Steel Construction, Chicago, IL.

AISC (2005b), *Seismic Provisions for Structural Steel Buildings*, ANSI/AISC 341-05, American Institute of Steel Construction, Chicago, IL.

AISC (2005c), *Specification for Structural Steel Buildings*, ANSI/AISC 360-05, American Institute of Steel Construction, Chicago, IL.

Astaneh, A. and Bergsma, G. (1993), "Cyclic Behavior and Seismic Design of Steel Base Plates," *Proceedings of Structures Congress*, ASCE, Vol. 1, pp. 409–414.

Bailey, J.W. and Burdette, E.G. (August 1977), "Edge Effects on Anchorage to Concrete," *Research Series No. 31*, Department of Civil Engineering, University of Tennessee, Knoxville, TN.

Ballio, G. and Mazzolani, F.M. (1983), *Theory and Design of Steel Structures,* Chapman and Hall, London and New York, pp. 257–264.

Baltay, P. and Gjelsvik, A. (1990), "Coefficient of Friction for Steel on Concrete at High Normal Stress," *Journal of Materials in Civil Engineering*, Vol. 2, No. 1, pp. 46–49.

Bažant, Z.P. (1984), "Size Effect in Blunt Fracture: Concrete, Rock, Metal," *Journal of Engineering Mechanics*, ASCE, Vol. 110, No.4, pp. 518–535.

Cannon, R.W., Burdette, E.G. and Funk R.R. (December 1975), "Anchorage to Concrete," *Report No. CEB 75-32*, Tennessee Valley Authority.

Cannon, R.W., Godfrey, D.A. and Moreadith, F.L. (1981), "Guide to the Design of Anchor Bolts and Other Steel Embedments," *Concrete International*, Vol. 3, No. 7, pp. 28–41.

Conrad, R.F. (1969), "Tests of Grouted Anchor Bolts in Tension and Shear," *Journal of American Concrete Institute*, Vol. 66, No. 9, pp. 725–728.

Cook, R.A. and Klingner, R.E. (1992), "Behavior of Multiple-Anchor Steel-to-Concrete Connections with Surface-Mounted Baseplates," *Anchors in Concrete: Design and Behavior*, SP-130, G.A. Senkiw and H.B. Lancelot III, Eds., ACI, Farmington Hills, MI, pp. 61–122.

DeWolf, J.T. (1978), "Axially Loaded Column Base Plates," *Journal of the Structural Division*, ASCE, Vol. 104, No. ST5, pp. 781–794.

DeWolf, J.T. and Ricker, D. (1990), *Design of Column Base Plates*, Steel Design Guide 1, American Institute of Steel Construction, Chicago, IL.

DeWolf, J.T. and Sarisley, E.F. (1980), "Column Base Plates with Axial Loads and Moments," *Journal of the Structural Division*, ASCE, Vol. 106, No. ST11, pp. 2167–2184.

Fenz, D. (2002), "Frictional Properties of Non-Metallic Materials for Use in Sliding Bearings: An Experimental Study," *Student Research Accomplishments 2001-2002*, Department of Civil, Structural and Environmental Engineering, University at Buffalo, NY, pp. 113–118.

Fisher, J.M. and Kloiber, L.A. (2006), *Base Plate and Anchor Rod Design*, Steel Design Guide 1, 2nd ed., AISC, Chicago, IL.

Fuchs, W., Eligehausen, R. and Breen, J.E. (1995), "Concrete Capacity Design (CCD) Approach for Fastening to Concrete," *ACI Structural Journal*, Vol. 92, No. 1, pp. 73–94.

Goldman, C. (1983), "Design of Column Base Plates and Anchor Bolts for Uplift and Shear," *Structural Engineering Practice*, Vol. 2, No. 2, pp. 103–115.

Gomez, I.R., Kanvinde, A.M., Smith, C. and Deierlein, G.G. (2009), "Shear Transfer in Exposed Column Base Plates," *Technical Report,* American Institute of Steel Construction, Chicago, IL.

Grauvilardell, J.E., Lee, D., Ajar, J.F. and Dexter R.J. (2005), "Synthesis of Design, Testing and Analysis Research on Steel Column Base Plate Connections in High Seismic Zones," *Structural Engineering Report No. ST-04-02*, Department of Civil Engineering, University of Minnesota, Minneapolis, MN.

Gresnigt, A.M., Romeijn, A., Wald, F. and Steenhuis, C.M. (2008), "Column Bases in Shear and Normal Force," *HERON*, Special issue: Steel Column Bases, Vol. 53, No. 1/2, pp. 87–108.

Hawkins, N.M. (1968), "The Bearing Strength of Concrete Loaded Through Rigid Plates," *Magazine of Concrete Research*, Vol. 20, No. 62, pp. 31–40.

Hill, R. and Siebel, M.P.L. (1951), "On Combined Bending and Twisting of Thin Tubes in Plastic Range," *Philosophical Magazine*, Vol. 42, No. 330, pp. 722–733.

Klingner, R.E., Mendonca, J.A. and Malik, J.B. (1982), "Effect of Reinforcing Details on the Shear Resistance of Anchor Bolts Under Reversed Cyclic Loading," *Journal of American Concrete Institute*, Vol. 79, No. 1, pp. 3–12.

Krawinkler, H., Gupta, A., Medina, R. and Luco, N. (2000), "Loading Histories for Seismic Performance Testing of SMRF Components and Assemblies," *Report No. SAC/BD-00/10*, SAC Joint Venture, Sacramento, CA.

MacGregor, J. and Wight, J.K. (2004), *Reinforced Concrete: Mechanics and Design,* 4th ed., Prentice-Hall, Upper Saddle River, NJ.

Nagae, T., Ikenaga, M., Nakashima, M. and Suita, K. (2006), "Shear Friction between Base Plate and Base Mortar in Exposed Steel Column Base," *Journal of Structural and Construction Engineering*, AIJ, No. 606, pp. 217–223. (In Japanese).

Nakashima, S. (1998), "Mechanical Characteristics of Exposed Portions of Anchor Bolts in Steel Column Bases under Combined Tension and Shear," *Journal of Constructional Steel Research*, Vol. 46, No. 1-3, Paper No. 277.

OSHA (2001), "Safety Standards for Steel Erection," *Occupational Safety and Health Administration*, Subpart R of 29 CFR Part 1926, Washington, D.C.

Ožbolt, J., Eligehausen, R., Periškić, G. and Mayer, U. (2007), "3D FE Analysis of Anchor Bolts with Large Embedment Depths," *Engineering Fracture Mechanics*, Vol. 74, No. 1-2, pp. 168–178.

Rabbat, B.G. and Russell, H.G. (1985), "Friction Coefficient of Steel on Concrete or Grout," *Journal of Structural Engineering*, Vol. 111, No. 3, pp. 505–515.

Rotz, J.V. and Reifschneider, M. (August 1989), "Combined Axial and Shear Load Capacity of Embedments in Concrete," *Proc. 10th International Conference, Structural Mechanics in Reactor Technology,* Anaheim, CA.

Shipp, J.G. and Haninger, E.R. (1983), "Design of Headed Anchor Bolts," *Engineering Journal*, AISC, Vol. 20, No. 2, pp. 58–69.

Tronzo, T.M. (1984), "Design of Heavy Steel Column Bases: Handling Lateral Forces—Some Practical Procedures," *Structural Engineering Practice*, Vol. 2, No. 4, pp. 279–300.